The 2019 World Congress on
Advances in Structural Engineering and Mechanics (ASEM19)
Jeju Island, Korea, September 17 - 21, 2019

Airflow over gable roof building with low roof slope: Wind tunnel experiment and CFD simulations

*Ruizhou Cao[1)], Zhixiang Yu[2)], Zhixiang Liu[3)], Xiaoxiao Chen[4)] and Fu Zhu[5)]

[1) ,2), 3), 4) 5)]*School of Civil Engineering, Southwest Jiaotong University, Chengdu 610031, China*
[1)] 15882354640@163.com

ABSTRACT

In this study, the levels of performance among there Reynolds-averaged Navier-Stokes equations (RANS) models (realizable k-ε model, RNG model and k-ω SST model) on the prediction of the flow characteristics above the low-sloped gable roof were examined. A measurement database of the time-averaged velocity, turbulent kinetic energy over a scaled model of 15° was conducted by particle image velocimetry (PIV). Sensitivity analyses for the turbulence models of the CFD simulations were performed. The result showed that the k-ω SST model exhibited the best performance due to the prediction of the vortex over the leeward roof. However, the realizable k-ε model and the RNG model both can't predict the existence of the vortex over the roof.

1. Introduction

Low-rise buildings are commonplace in cities and villages. Due to the complexity of the turbulent motion at the bottom of the atmospheric boundary layer, the flow characteristics around low-rise buildings become very complicated. This complexity makes it difficult to predict wind loads and wind conditions around low-rise buildings. Gable roof is commonplace in low-rise buildings, of which roof slope varies from 0 to 70 (Taylor, 1980). Due to the effect of the roof slope, the aerodynamic characteristics around gable-roof buildings is different from the cubic buildings(Sousa and Pereira, 2004). In the past few decades, the wind tunnel tests(Cope et al., 2005; Kanda and Maruta, 1993; O'Rourke et al., 2004) case histories analysis(O'Rourke and Auren, 1997; Thiis and O'Rourke, 2015) and the CFD simulations(Ozmen et al., 2016; Tominaga et al., 2015; Xing et al., 2018b; Zhou et al., 2019) are extensively used to investigate the flow characteristics around the gable-roof buildings. However, due to the limitations of testing and analysis techniques and the complex variations in roofing slopes, the current research on this issue is still insufficient.

With the development of computer technology, numerical simulation method combined with wind tunnel test has become an effective tool to study the flow properties around the buildings. To confirm the applicability of CFD analyses, the validation and verification processes are crucial. From previous literature, the model with median roof slope, such as 26.7° (Tominaga et al., 2015) or 30° (Zhou et al., 2019), seem to be the best choice when used to verify the accuracy of the simulation results in the study of

slope influence. However, based on the numerical simulation results of the realizable k-ε turbulence model, Zhou et al. (2019) indicated that the critical slope for the flow field change is between 20° and 25°. From the distribution of wind streamlines by Xing et al. (2018) , Significant differences in flow characteristics of the 11.3° roof and 31°roof are observed, which are significantly greater than the difference between the 30° roof and the 50° roof (Zhou et al., 2019). Similarly, Tominaga et al. (2015) clarified that the difference of the flow field properties between the 16.7° roof and 26.7° roof is greater than that between the 26.7° and 36.7° roofs. Although the above conclusions are different, they all emphasize that the change of airflow characteristics around the low-sloped roofs is more significant with the increase of roof slope, and the performance of turbulence models for the airflow characteristics above the low-slope roof remains to be examined.

Based on the above description, the PIV wind tunnel experiment and CFD simulations were carried out. Firstly, the average velocity and the turbulent kinetic energy distribution above the gable roof of 15° were accurately captured by the PIV wind tunnel test. Next, the sensitivity analyses for the performance of the RANS turbulence models were discussed. In this paper, Section 2 introduces a detailed description of the PIV wind tunnel test and CFD simulation settings. Section 3 introduces the discussions on the sensitivity analyses for turbulence models.

2. Test models and methods

2.1 model design

The Dimensions of the gabled roof building model of this experiment is shown in Figure 1. The geometric scaling ratio is 1/100. The model is constructed from plywood with smooth surfaces, and the surface is sprayed with black matte paint to reduce the light scattering during PIV test. Limited by PIV test equipment, its imaging size is up to 250 mm. The model characteristic height, denoted as *H*, is set as 75 mm.

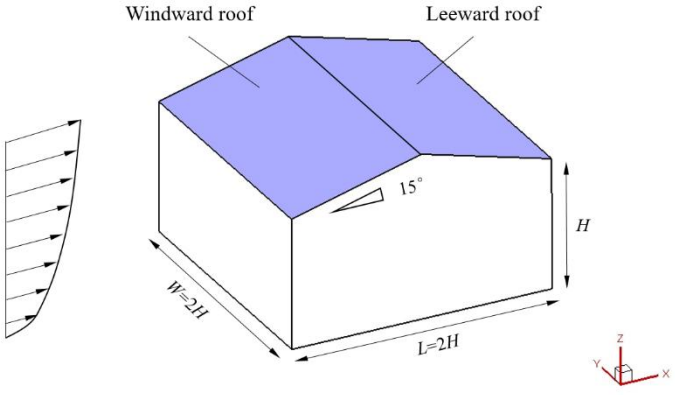

Fig. 1 Dimensions of gabled roof building model

2.2 PIV experiment

The experiment is carried out in a closed-circuit wind tunnel at Xihua University.

The dimension of the test section is 3 m(x)×1.2 m(y)×1.2 m(z), in which the wind velocity can reach 60 m/s. The test section is shown in Fig. 2, where glass is installed on the sides and top. A combination of spires and rough elements is used to conduct the mean wind velocity profile. The nominal wind velocity is set to 8.15 m/s. Fig. 3 shows profiles of mean wind velocity obtained by the test measurement, in which the mean wind velocity is dimensionless by the wind velocity $U(H)$ at the reference height of the eaves.In the experiment, the cobra three-dimensional pulsating anemometer is used to measure the mean wind velocity and turbulent intensity, of which the sampling frequency is 256 Hz and the sampling time is 60 s. The PIV test system adopts the German PIVTEC high-resolution particle image velocity measurement system, which includes high-speed CMOS camera, synchronizer, laser generator (with a wavelength of 532 nm), laser sheet generator, tracer particles delivery device and computer (shown in Fig. 1(a)).

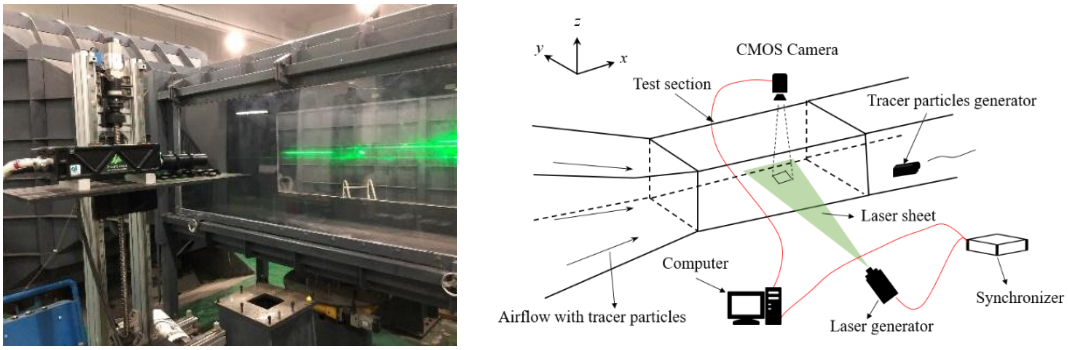

（a）Test section （b）PIV system

Fig. 2 Diagram of the PIV system

（a）mean wind velocity profile （b）turbulent intensity

Fig. 3 Profiles of mean wind velocity

2.3 Computational methods

In this paper, the realizable k-ε (Shih et al., 1995), the RNG k-ε (Yakhot et al., 1992)

and the k-ω SST (Menter, 1994) turbulence models in the commercial CFD software ANSYS/Fluent are used. The simulation model is the same with the test model, and according to recommendations of best practice guidelines, the computational domain size of the flow field is 16 *L*(*x*) × 11 *W*(*y*) × 10 *H*(*z*), as shown in Fig. 4. Hexahedral elements are mainly used to create the mesh cooperating with tetrahedral and prism solid elements. The minimum size of the compute grid for the realizable k-ε model and the RNG model is 0.0021 m, and the total number of grids is 710285. For the k-ω SST model, additional prism elements are imposed near solid boundaries to capture boundary layers, of which the minimum mesh height is set as 1.2×10^{-5}, and the total number of grids is 1005404. The grid details are shown in Fig. 5.

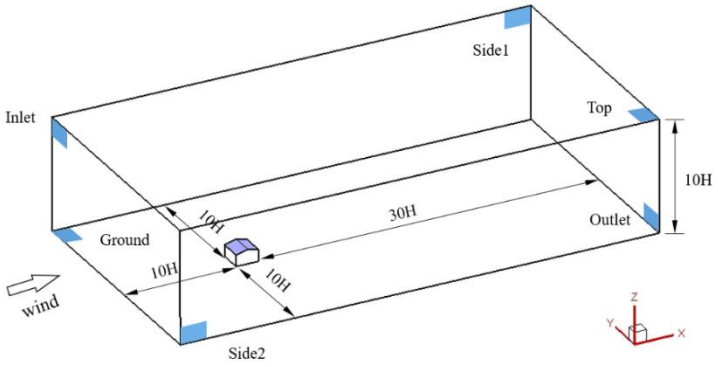

Fig. 4 The dimensions of the computational domain

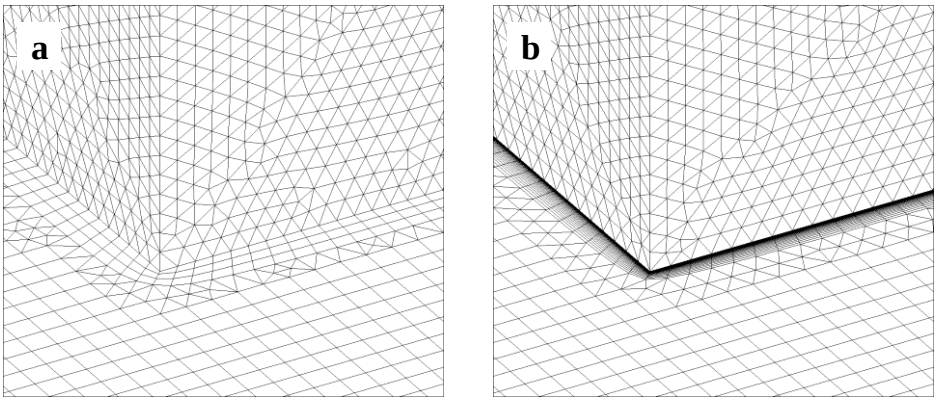

Fig. 5 Mesh details: (a) RKE/RNG model, (b) k-ω SST model,

An atmospheric wind profile is used in numerical simulation. The mean profile of wind velocity is measured in the wind tunnel experiment, and described as follows:

$$U(z)=\frac{u_*}{\kappa}\ln(\frac{z}{z_0}+1) \quad (1)$$

where u_* is the friction velocity, κ is von Karman constant 0.42，z_0 is the roughness height 0.000205 m, fitted through the data from the wind tunnel measurement. The inlet turbulence kinetic energy, calculated by the measured turbulence intensity and the mean wind velocity, is expressed as follows:

$$k(z) = a(I_u(z)u(z))^2 \quad (2)$$

where $I_u(z)$ is the turbulence intensity, $u(z)$ is the mean wind velocity at the height of z, parameter a is taken as 1.5 in this paper.

The turbulence dissipation rate is given in Equation (3) and the specific dissipation rate in Equation (4),

$$\varepsilon(z) = \frac{u_*^3}{\kappa(z + z_0)} \quad (3)$$

$$\omega(z) = \frac{\varepsilon(z)}{C_\mu k(z)} \quad (4)$$

The roughness height, denoted as k_S, is calculated by the ground roughness height and roughness constant, and is shown below：

$$k_S = \frac{9.793 z_0}{C_S} \quad (5)$$

where C_S is the roughness constant, taken as 1.0 in this paper.

Boundary conditions and solver settings for all cases are summarized. Symmetry boundary conditions are imposed at the top and sides surfaces, meaning zero normal velocity and zero gradients for all the variables at these boundaries. The ground surface and model surfaces are set as no-slip walls, where the standard wall functions are used for the RKE and RNG model. the value of k_S for the ground surface is calculated as 0.002 m and is set as 0 m for the model surface. The outlet condition is imposed with zero static pressure. In addition, the SIMPLE algorithm is used for pressure-velocity coupling and all transport equations are discretized using a second-order upwind scheme.

3. Comparison of the results obtained by CFD and experiment

The averaged y+ value of 40 is used for RKE/RNG models (Tominaga et al., 2015), and the averaged y+ value of 0.2 is used for k-ω SST model (Bardina et al., 1997). Fig.6

shows the comparison of the measured data with the results of the three turbulence models. As can be seen from the left, the RKE model and RNG model have a poor velocity prediction over the leeward roof of 15°, while the k-ω SST model is more accurate at velocity prediction. From the right graph, it can be seen that the turbulence energy above the windward roof obtained with RKE model is too large compared with that obtained with the RNG model and the k-ω SST model. On the leeward surface, due to the different treatment for wall surface, the RKE/RNG model is more accurate in predicting turbulence energy in the near-wall area, while the calculation value obtained with the k-ω SST model is relatively small. However, for the area away from the wall, the prediction accuracy of the k-ω SST model is better than that of the RKE/RNG model.

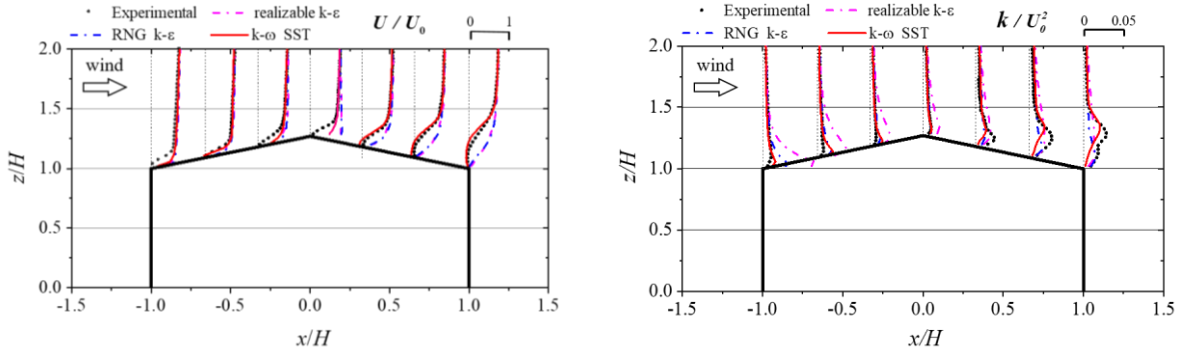

Fig. 6. Comparison, with measured values, of streamwise velocity and turbulent kinetic energy k, obtained with different turbulence models.

Fig.7 shows the distributions of streamlines obtained with three turbulence models and PIV data. It can be seen that the k-ω SST model is too sensitive to the vortex prediction above the leeward surface, and the initial position prediction for the reverse flow is relatively ahead, while the RKE/RNG model cannot predict the vortex above the leeward surface of 15°. Ozmen et al. (2016) stated that the largest values of turbulence kinetic energy behind the roof ridge of the gable roof occurs in the mixing layer between the free stream flow and reverse flow region, and the appearance of the upper vortex on the leeward surface increases the turbulence intensity. Although the k-ω SST model has a low prediction of turbulent energy in the near-wall area, The good prediction of the vortex makes the prediction of turbulent energy obtained with k-ω SST model closer to the measurement data than that obtained with the RKE/RNG model for the area far from the roof.

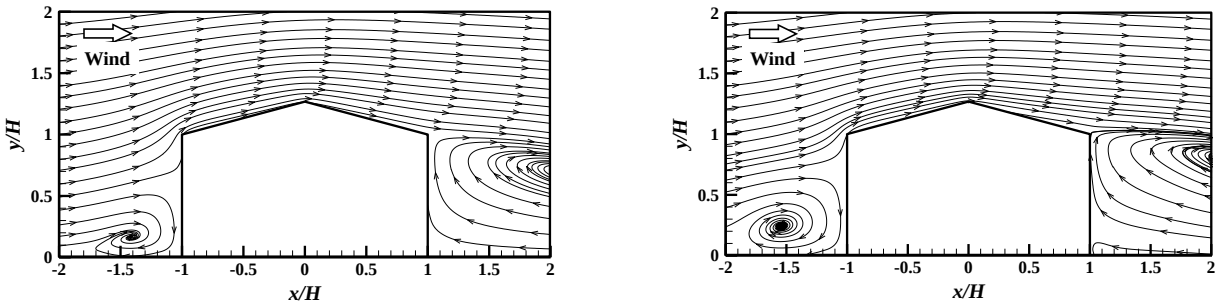

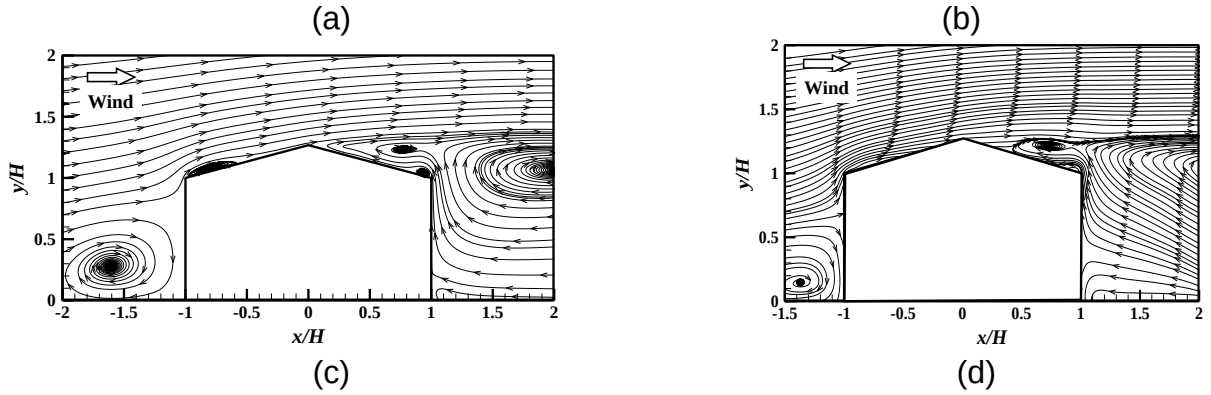

Fig. 7 Streamlines: (a) RKE model, (c) k-ω SST model, (d) PIV data

To quantify the agreement between computed and measured results, two validation metrics are used in this paper, respectively:

(a) The factor of 2 (FAC2) showed the fraction of the simulated results in a factor of two of the corresponding measured results. It was bounded on the interval [0, 1] and indicated an overall performance of the model with infrequently occurring strong over- or under-predictions.

$$FAC2 = \frac{1}{N}\sum_i F_i \qquad F_i = \begin{cases} 1, if\ \frac{1}{2} \le \frac{P_i}{M_i} \le 2 \\ 0, \text{else} \end{cases}$$

(6)

(b) The modified normalized mean bias (MNMB) indicated the tendency of the turbulence model's over-/under-predictions with the interval [-2, 2].

$$MNNM = \frac{2}{N}\sum_i \left(\frac{P_i - M_i}{P_i + M_i} \right)$$

(7)

The computational results of the metrics are listed in Table 1. The results obtained with RKE model are very close to those obtained with the RNG model in terms of velocity prediction, but the RNG model has better prediction ability for turbulence intensity than the RKE model. From the results of the three turbulence models, the SST model exhibits the highest level of performance in the simulation of flow characteristics above the gable roof of 15°.

Table 1 Validation metrics

	U/U_0		k/U_0^2	
	FAC2	MNMB	FAC2	MNMB
RKE	0.789	0.424	0.181	0.822
RNG	0.789	0.419	0.637	0.327

SST	0.856	0.249	0.809	0.216

4. Conclusions

In this paper, the PIV wind tunnel experiment and numerical simulations are carried out, and the conclusions are as follows:

(1) Detailed distributions of the time-averaged velocity, turbulent kinetic energy above the low-sloped gable roof were established as a validation database for CFD.

(2) The k-ω SST model exhibits the highest accuracy for the prediction of flow field above the low-sloped gable roof due to the prediction of the vortex over the leeward roof.

the realizable k-ε model and the RNG model both can't predict the exsitance of the vortex over the roof.

References

Bardina, J., Huang, P., Coakley, T., Bardina, J., Huang, P. and Coakley, T., 1997. Turbulence modeling validation, 28th Fluid dynamics conference, pp. 2121.

Blocken, B. (2015), "Computational Fluid Dynamics for urban physics: Importance, scales, possibilities, limitations and ten tips and tricks towards accurate and reliable simulations." Build. Environ. , Vol. 91, 219-245.

Cope, A.D., Gurley, K.R., Gioffre, M. and Reinhold, T.A. (2005), "Low-rise gable roof wind loads: Characterization and stochastic simulation." J. Wind Eng. Ind. Aerodyn. , Vol. 93(9), 719-738.

Kanda, M. and Maruta, E. (1993), "Characteristics of fluctuating wind pressure on long low-rise buildings with gable roofs." J. Wind Eng. Ind. Aerodyn. , Vol. 50, 173-182.

Menter, F.R. (1994), "Two-equation eddy-viscosity turbulence models for engineering applications." Aiaa J, 32(8), 1598-1605.

O'Rourke, M. and Auren, M. (1997), "Snow loads on gable roofs." J. Struct. Eng., Vol. 123(12), 1645-1651.

O'Rourke, M., DeGaetano, A. and Tokarczyk, J.D. (2004), "Snow drifting transport rates from water flume simulation." J. Wind Eng. Ind. Aerodyn. , Vol. 92(14-15), 1245-1264.

Ozmen, Y., Baydar, E. and van Beeck, J.P.A.J. (2016), "Wind flow over the low-rise building models with gabled roofs having different pitch angles." Build. Environ. , Vol. 95, 63-74.

Shih, T.-H., Liou, W.W., Shabbir, A., Yang, Z. and Zhu, J. (1995), "A new k-ϵ eddy viscosity model for high reynolds number turbulent flows." Comput. Fluids., Vol. 24(3), 227-238.

Sousa, J.M.M. and Pereira, J.C.F. (2004), "DPIV study of the effect of a gable roof on the flow structure around a surface-mounted cubic obstacle." Exp. Fluids., Vol. 37(3), 409-418.

Taylor, D.A. (1980), "Roof snow loads in Canada." Can. J. Civ. Eng. , Vol. 7(1), 1-18.

Thiis, T.K. and O'Rourke, M. (2015), "Model for snow loading on gable roofs." J. Struct. Eng., Vol. 141(12), 04015051.

Tominaga, Y., Akabayashi, S.-i., Kitahara, T. and Arinami, Y. (2015), "Air flow around isolated gable-roof buildings with different roof pitches: Wind tunnel experiments and

CFD simulations." Build. Environ., Vol. 84, 204-213.
Tominaga, Y., Mochida, A., Yoshie, R., Kataoka, H., Nozu, T., Yoshikawa, M. and Shirasawa, T. (2008), "AIJ guidelines for practical applications of CFD to pedestrian wind environment around buildings." J. Wind Eng. Ind. Aerodyn. , Vol. 96(10-11), 1749-1761.
Xing, F., Mohotti, D. and Chauhan, K. (2018), "Study on localised wind pressure development in gable roof buildings having different roof pitches with experiments, RANS and LES simulation models." Build. Environ., Vol. 143, 240-257.
Yakhot, V., Orszag, S., Thangam, S., Gatski, T. and Speziale, C., 1992. Development of turbulence models for shear flows by a double expansion technique. Phys. Fluids., Vol. 4(7), 1510-1520.
Zhou, X., Kang, L., Gu, M., Qiu, L. and Hu, J. (2016), "Numerical simulation and wind tunnel test for redistribution of snow on a flat roof." J. Wind Eng. Ind. Aerodyn. , Vol. 153, 92-105.
Zhou, X., Zhang, Y., Kang, L. and Gu, M. (2019), "CFD simulation of snow redistribution on gable roofs: Impact of roof slope." J. Wind Eng. Ind. Aerodyn. , Vol. 185, 16-32.
Zhu, F., Yu, Z., Zhao, L., Xue, M. and Zhao, S. (2017), "Adaptive-mesh method using RBF interpolation: A time-marching analysis of steady snow drifting on stepped flat roofs." J. Wind Eng. Ind. Aerodyn. , Vol. 171, 1-11.